

Article

Antibacterial Activity of Ulva/Nanocellulose and Ulva/Ag/Cellulose Nanocomposites and Both Blended with Fluoride against Bacteria Causing Dental Decay

Ragaa A. Hamouda ^{1,2,*} , Fauzia A. K. Qarabai ¹, Fathi S. Shahabuddin ³, Turki M. Al-Shaikh ¹ and Rabab R. Makharita ^{1,4} 

¹ Department of Biology, College of Sciences and Arts at Khulis, University of Jeddah, Jeddah 21959, Saudi Arabia

² Department of Microbial Biotechnology, Genetic Engineering and Biotechnology Research Institute (GEBRI), University of Sadat City, Sadat City 32897, Egypt

³ Harad Center Makkah Ministry of Health, Riyadh 24342, Saudi Arabia

⁴ Botany and Microbiology Department, Faculty of Science, Suez Canal University, Ismailia 41522, Egypt

* Correspondence: ragaahom@yahoo.com

Abstract: One of the most prevalent chronic infectious disorders is tooth decay. Acids produced when plaque bacteria break down sugar in the mouth cause tooth decay. *Streptococcus mutans* and *Lactobacillus acidophilus* are the most prominent species related to dental caries. Innovative biocidal agents that integrate with a biomaterial to prevent bacterial colonization have shown remarkable promise as a result of the rapid advancement of nanoscience and nanotechnology. In this study, *Ulva lactuca* was used as a cellulose source and reducing agent to synthesize nanocellulose and Ulva/Ag/cellulose/nanocomposites. The characterizations of nanocellulose and Ulva/Ag/cellulose/nanocomposites were tested for FT-IR, TEM, SEM, EDS, XRD, and zeta potential. Ulva/Ag/cellulose/nanocomposites and Ulva/nanocellulose, both blended with fluoride, were tested as an antibacterial against *S. mutans* ATCC 25175 and *L. acidophilus* CH-2. The results of the SEM proved that nanocellulose is filament-shaped, and FT-IR proved that the functional groups of Ulva/nanocellulose and Ulva/Ag/cellulose/nanocomposites and cellulose are relatively similar but present some small diffusion in peaks. The TEM image demonstrated that the more piratical size distribution of Ulva/Ag/cellulose/nanocomposites ranged from 15 to 20 nm, and Ulva/nanocellulose ranged from 10 to 15 nm. Ulva/Ag/cellulose/nanocomposites have higher negativity than Ulva/nanocellulose. Ulva/Ag/cellulose/nanocomposites and Ulva/nanocellulose possess antibacterial activity against *S. mutans* ATCC 25175 and *L. acidophilus* CH-2, but Ulva/Ag/cellulose/nanocomposites are more effective, followed by that blended with fluoride. It is possible to use Ulva/Ag/cellulose/nanocomposites as an antimicrobial agent when added to toothpaste. It is promising to discover an economic and safe nanocomposite product from a natural source with an antimicrobial agent that might be used against tooth bacteria.

Keywords: *Ulva lactuca*; *S. mutans* ATCC 25175; *L. acidophilus* CH-2; cellulose; nanocellulose



Citation: Hamouda, R.A.; Qarabai, F.A.K.; Shahabuddin, F.S.; Al-Shaikh, T.M.; Makharita, R.R. Antibacterial Activity of Ulva/Nanocellulose and Ulva/Ag/Cellulose Nanocomposites and Both Blended with Fluoride against Bacteria Causing Dental Decay. *Polymers* **2023**, *15*, 1047. <https://doi.org/10.3390/polym15041047>

Academic Editor: Francesca Ferrari

Received: 11 January 2023

Revised: 13 February 2023

Accepted: 15 February 2023

Published: 20 February 2023



Copyright: © 2023 by the authors. Licensee MDPI, Basel, Switzerland. This article is an open access article distributed under the terms and conditions of the Creative Commons Attribution (CC BY) license (<https://creativecommons.org/licenses/by/4.0/>).

1. Introduction

One of the most significant problems in public health is tooth decay [1]. General health is affected by oral health [2]. Dental caries is related to behavioral, economic, and social aspects and increases the incidence of diseases among people [3]. Dental caries is a bacterial illness that gradually arises from complicated biological interactions between acidogenic bacteria and fermentable carbohydrates [4]. Acids from bacterial metabolism that diffuse into enamel and dentine generate the bacterial disease process known as dental caries, which is contagious [5]. Worldwide, 36% of people suffer dental caries in their adult teeth (Gram-positive bacteria creating tooth decay) [6]. Dental caries is caused by

Streptococcus mutans, and this requires that the organism can build biofilms and create acid on the tooth surface [7]. These bacteria are extremely acidogenic, creating short-chain acids that tenderize the hard tissues of teeth [8]. They adhere tightly to the surface of the teeth by synthesizing insoluble carbohydrates with three isozymes of glucosyl transferases, catalyzing and metabolizing sucrose [9]. *Streptococcus mutans* and Lactobacilli are most connected with dental caries [10]. Dental caries and necrotizing fasciitis are just two of the illnesses that streptococci can cause (ibid.). They are the sole bodily portion that is not subject to metabolic change; tooth surfaces are special [11].

Nanotechnology is significant in biomedical applications as a different antimicrobial strategy due to the recurrence of diseases and antibiotic-resistant bacteria [12]. The development of a new area dubbed “nano dentistry” is being fueled by the rising interest in dental uses of nanotechnology [13]. Furthermore, nanoparticles have antimicrobial coatings and films as alternative methods to prohibit biofouling [14].

A linear polysaccharide polymer known as cellulose is found in various biomasses, including cotton, trees, tunicates, algae, plants, and trees [15]. Green algae are the best natural source for extracting cellulose [16]. Cellulose can be processed chemically, mechanically, or enzymatically to create nanocellulose [17]. Nanocellulose is made up of 1:100 nm-sized cellulose fibrils [18].

Cellulose nanofiber (NFC), also referred to as nanocellulose, is a rapidly developing source of “green technology”, “recyclable”, “renewable”, “eco-friendly”, “triggered biodegradable”, and “sustainable” materials [19]. Nanocellulose is preferable to cellulose due to its high aspect ratio and large surface area [20]. Nanocellulose is divided into three classes: nanocrystalline celluloses (CNC), nanofibrillated celluloses (NFC), and bacterial celluloses (BC) [21]. These three divisions are based on sources, functions, modes of production, structures, and reaction conditions [22]. Nanocellulose has become widely used in many applications due to its good mechanical properties, renewable susceptibility, and role in improving composites [23]. Due to its biocompatibility, biodegradability, and nontoxicity, nanocellulose is used as an antimicrobial in biomedical applications [24].

Cellulose nanofibers are used to produce nanocomposites from inorganic compounds due to their high specific surface area and small size [25]. ZnO/CNC presented enhanced antibacterial activity when compared with pure ZnO against both *S. aureus* and *E. coli* [26]. Moreover, ZnO/BC composites have demonstrated vigorous antibacterial activity against *S. aureus* and *E. coli* [27]. Synthesized Ag@AgCl-reinforced cellulose composites demonstrated enhanced antibacterial activities [28]. Fe₃O₄/Ag@NFC nanocomposites can also be employed in medicinal applications as an antibacterial substance [29]. Nanocomposites consist of cellulose, AgCl, and Ag successfully synthesized with excellent antimicrobial properties [30].

Fluoride has been used to prevent cavities for about forty years, and during the past twenty years, it has been used more widely [31]. Fluoride works by three mechanisms to prevent decay: inhibiting bacterial enzymes, reinforcing remineralization at crystal surfaces, and preventing purification on crystal surfaces [32]. Proper use of fluoride improves oral health and promotes general health [33]. In the late 1970s, the first signs of fluoride’s positive effect on children’s dental health appeared in the UK [34]. The daily utilization of fluoride toothpaste is a major reason for the decline in the rate of caries around the world [35]. Persistent low-level treatments of fluoride are more effective in caries protection than rare usage of high-level treatments [36]. The status of water fluoridation in caries prohibition is obvious around the world [37].

This research aims to extract cellulose from marine alga (*Ulva lactuca*), synthesize cellulose nanoparticles, and perform biosynthesis of Ulva/Ag/cellulose nanocomposites. Furthermore, it aims to investigate the antibacterial activities of cellulose nanoparticles and Ulva/Ag/cellulose nanocomposites and both blended with fluoride to provide reinforcement against *Streptococcus mutans* and *Lactobacillus acidophilus*, which cause tooth decay.

2. Materials and Methods

2.1. Materials

The materials used in the study were green alga (*Ulva lactuca*), sodium hydroxide (NaOH), ethanol (99%), hydrochloric acid (37%), hydrogen peroxide (6%), silver nitrate 99.9+% (metals basis), and distilled water. All the chemicals used in this research were of analytical grade and applied without further purification. Chemical materials were purchased from the Saudi Chemical company (PanReac AppliChem, Ar Riyad, Saudi Arabia).

2.2. Alga Collection

Alga was collected from the Red Sea shore in Jeddah, Saudi Arabia (21°38'43.4'' N 39°06'04.7'' E). To remove impurities, alga was rinsed in water and then dried in an oven set to 60 °C. Crushed and sieved dry samples were used.

2.3. Extracting Cellulose from *U. lactuca* Green Alga

Ulva lactuca (50 g) was milled to a soft powder. After that, 50 g of grounded alga was placed in a flask with 170 mL of pure ethanol and 30 mL of water for 6 h over heat at 60 °C with a magnet (stirring) and filtered, and the liquid phase was discarded. The insoluble fraction was repeatedly cleaned with 99% ethanol before being dried for 16 h at 37 °C in the oven. After drying, the sample was further processed by suspending it in 400 mL of 4% H₂O₂, which was then heated to 80 °C for 16 h to remove any remaining green pigments and other colored impurities. The mixture was filtered, and the liquid phase was discarded after cooling to room temperature. The insoluble fraction was then suspended in 400 mL of 0.5 M Na OH after being rinsed with distilled water. For 16 h, the mixture was maintained at 60 °C and was then taken out of the oven, allowed to cool to room temperature, filtered, and washed three times with distilled water before the insoluble fraction was collected.

2.4. Extraction of Nanocellulose

The extracted cellulose was treated with 27 mL HCl and 173 mL of distilled water at 90 °C for 10 min. The combination was filtered by removing the liquid phase after cooling to room temperature, and the insoluble fraction was then cleaned with distilled water. When the mixture was entirely dry, it was stored at 60 °C.

2.5. Synthesis *Ulva/Ag/Cellulose* Nanocomposite

2.5.1. Preparation of Silver Nanoparticles

Algal Extract

Dry alga *Ulva lactuca* (1 g) was added to 100 mL distilled water, boiled for 1 h, and then filtered.

Biosynthesis of Ag Nanoparticles

Silver nitrate (0.17 g) was added to 90 mL of distilled water. The prepared alga extract (10 mL) was added drop-wise to the solution at 60 °C with constant stirring until the mixture turned brown.

2.5.2. Biosynthesis of *Ulva/Ag/Cellulose* Nanocomposites

Silver nitrate (0.085 g) was added to 45 mL of distilled water, then different concentrations of nanocellulose (0.1, 0.2, 0.4, and 0.8 g) were added separately, and then alga extract (5 mL) was added as drops. The solution was heated at 60 °C and stirred until the color changed to brown.

2.5.3. Biosynthesis of *Ulva/Nanocellulose*, *Ulva/Ag/Cellulose* Nanocomposites, and Both Blended with Fluoride

Silver nanoparticles (1.7 mg/mL) were synthesized by *U. lactuca*, 2 mg/mL *Ulva/nanocellulose*, and 2 mg/mL *Ulva/Ag/cellulose* nanocomposites, and 1 mL of each was blended with 10 mL fluoride (1.23%) by magnetic stirrer for 10 min.

2.6. Characterization

2.6.1. Fourier Transform Infrared (FT-IR)

Ulva/cellulose and Ulva/Ag/cellulose nanocomposite functional groups were examined using a Fourier transform infrared spectrometer (FT-IR), Thermo Fisher Nicolet IS10, (Waltham, MA, USA) Spectrometer, FT-IR spectrum ranged between 4000 and 400 cm^{-1} .

2.6.2. Scanning Electron Microscope (SEM)

The morphologies of Ulva/nanocellulose and Ulva/Ag/cellulose nanocomposite were examined using scanning electron microscopy (SEM) operating at 30 kV (SEM, JEOL JSM-6510/v, Tokyo, Japan).

2.6.3. Transmission Electron Microscopy (TEM)

The morphology of synthesized Ulva/nanocellulose and Ulva/Ag/cellulose nanocomposite were examined using TEM (JEOL JSM-6510/v, Tokyo, Japan) at the nanoscale.

2.6.4. X-ray Powder Diffraction (XRD)

X-ray diffraction patterns of Ulva/nanocellulose and Ulva/Ag/cellulose nanocomposite were analyzed using an X-ray diffractometer (PAN Analytical X-Pert PRO, spectris plc, Almelo, The Netherlands). The cellulose size was determined using Scherrer's equation.

$$\text{Crystal Size } L = \lambda k / c \beta \theta$$

where $\lambda = 0.1540 \text{ nm}$, k is the constant factor of 0.91, θ = diffraction angle in radians, and β = full width at half maximum (FWHM).

2.6.5. Energy-Dispersive Spectroscopy (EDS)

A field emission scanning electron microscope equipped with energy-dispersive spectroscopy (EDS) (JEOL JSM-6510/v, Tokyo, Japan) was used to investigate the surface morphology of the Ulva/nanocellulose and Ulva/Ag/cellulose nanocomposite.

2.6.6. Zeta Potential Analysis

The zeta potential of the Ulva/nanocellulose and Ulva/Ag/cellulose nanocomposite provides details of the stabilization in the middle of the liquid that it is dispersed in (Malvern Zeta size Nano-Zs90, Malvern, PA, USA).

2.6.7. Differential Scanning Calorimetry (DSC)

Differential scanning calorimetry DSC testing 19 mg of Ulva/Ag/cellulose nanocomposite blend with fluoride was conducted using differential scanning calorimeter DSC131 EVO France.

2.7. Antibacterial Activities

The agar-well diffusion technique was used to study the antibacterial properties of hybrids made of AgNPs, Ulva/nanocellulose, and Ulva/Ag/cellulose nanocomposite, and both blended with fluoride against *S. mutans* ATCC 25175 and *L. acidophilus* CH-2 [38] as model Gram-positive bacteria associated with dental caries. Muller–Hinton agar was poured into a Petri dish and solidified. The turbidity of an overnight broth culture of *S. mutans* ATCC 25175 and *L. acidophilus* CH-2 was adjusted to 0.5 McFarland standards. Then, 50 μL of bacterial suspension was spread over the plates separately using a sterilized cotton swab. After that, 100 μL of the prepared nanoparticles at different concentrations of nanocellulose (0.2, 0.4, 0.8, and 1.6%) was applied to 0.7 mm-diameter wells on each bacterial agar plate. Plates were incubated at 37 $^{\circ}\text{C}$ for 24 h. The inhibitory zone (mm) was recorded. The experiment was conducted in triplicate.

2.8. Minimum Inhibitory Concentration (MIC)

The minimum inhibitory concentration (MIC) of Ulva/Ag/cellulose nanocomposite was examined using the standard broth dilution method at diverse concentrations oscillating from 0.002 to 0.00005 g/mL. Mueller–Hinton agar (MHA) medium was prepared and inoculated under aseptic conditions with 50 μ L of the overnight bacteria suspension and allowed to dry. Wells were filled with 100 μ L of different serial dilutions of Ulva/Ag/cellulose nanocomposite separately. After 24 h of incubation at 37 $^{\circ}$ C, plates were checked to see if an inhibition zone (mm) had formed around each well.

2.9. Statistical Analysis

Data were obtainable as mean \pm SEM, and SPSS 16 was used for the statistics, together with one-way ANOVA.

3. Results and Discussion

3.1. FT-IR Spectroscopy Analysis

Figure 1 and Table 1 show the results of the FT-IR spectroscopy analysis of cellulose, nanocellulose, and Ulva/Ag/cellulose nanocomposite derived from *U. lactuca*. The results demonstrate that 9 peaks were obtained with cellulose, 18 peaks with nanocellulose, and 11 peaks with Ag/Ulva cellulose nanocomposites. The results investigated the modification of numbers and positions (wavenumbers) and demonstrated the differences in the chemical structure of each compound.

Table 1. Tabulated absorption peaks assigned to the active groups of cellulose (A), nanocellulose (B), and Ulva/Ag/cellulose nanocomposites (C).

Wavenumber cm^{-1}	A	B	C	Active Groups	References
3508	D	ND	ND	O-H stretching	[39,40]
3413	ND	D	+6	symmetric NH_2	[41]
2924	D	ND	+4	C-H stretching	[42,43]
2851	D	+6	ND	CH_2 symmetric	[44]
1718	ND	D	ND	C=O	[45]
109	ND	D	ND	C=O stretching	[46]
1656	D	ND	ND	Amide I	[47]
1638	D	−3	+1	amide I	[43,48]
1545	ND	D	+3	Peptide amide II	[49]
1529	ND	D	ND	amide II	[50]
1427	D	−24	ND	CH_3	[51]
1382	ND	D	+2	CH bending vibrations	[52]
1233	ND	D	+1	PO ₂ -asymmetric	[53]
1197	ND	D	ND	carbohydrates	[54]
1159	ND	D	+1	(C-C/C-N stretching)	[55,56]
1114	ND	D	ND	O-H association band	[57]
1037	D	+36	+36	C=O stretch	[51]
848	D	ND	ND	C-H	[58]
793	D	ND	ND	C-C bond	[59]
669	ND	D	D	C-H bending	[60]
607	D	−5	−5	$\text{C}\equiv\text{C-H}$	[61]
528	ND	D	D	C-S stretching	[61,62]

D: Detected, ND: Not Detected, (−): shifted wavenumber by minus, (+) shifted wavenumber by addition.

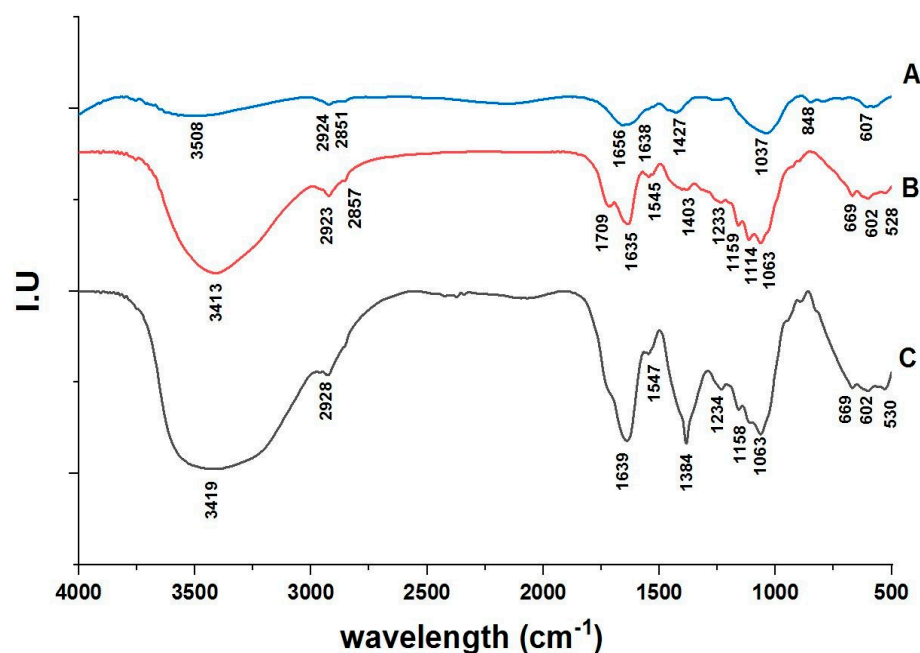
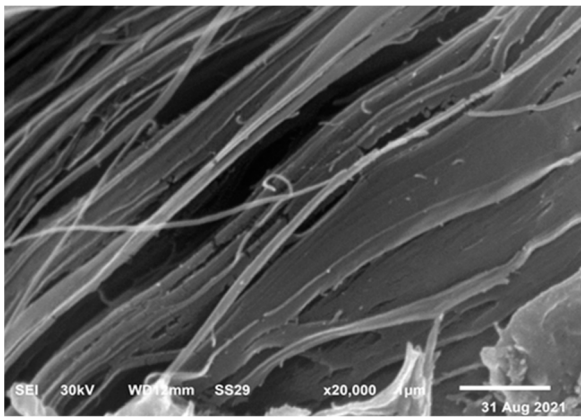


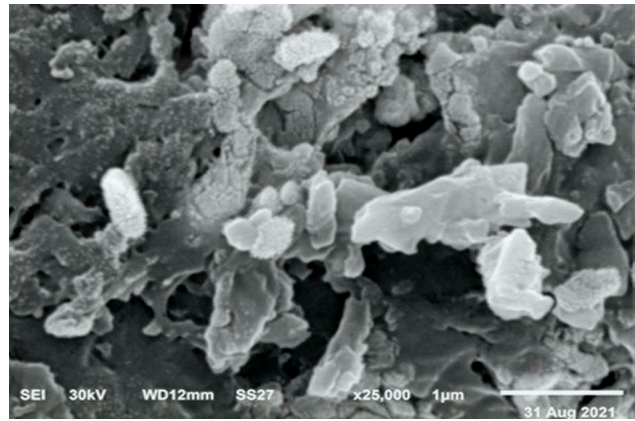
Figure 1. FT-IR spectroscopy of Ulva cellulose (A), Ulva nanocellulose (B), and Ag/Ulva cellulose nanocomposites (C).

3.2. SEM and TEM Images

Figure 2a displays SEM (scanning electron microscope) images of the surface of nanocellulose extracted from *U. lactuca*. The image showed that nanocellulose extracted from *U. lactuca* comprises filaments, a result proved by Xiang et al. [63] who reported that the SEM imagery of *Cladophora glomerata* nanocellulose comprises filaments. Peng et al. [64] demonstrated that nanocellulose is arranged in a fiber network. The SEM image of Ulva/Ag cellulose nanocomposites indicates ridges and valley surfaces (Figure 2b), which confirmed a highly organized by layer porous architecture and large surface area. These results are confirmed by Tan [65], who reported that, after the addition of Ag rough, nonhomogeneous Turing structures increased. Figure 3a–b shows TEM images of biosynthesized nanocellulose and Ulva/Ag/cellulose nanocomposites derived from *U. lactuca*. The morphological studies of Ulva nanocellulose indicate a polydispersive and spherical shape and the major range size is from 10 to 15 nm (Figure 4a). The fine particle size will result in a large surface area that will enhance the nanoparticles' catalytic activity. The results appeared in TEM images of Ulva/Ag/cellulose nanocomposites that are polydispersed hexagonal-shaped nanoparticles with sizes ranging from 5 to 38.1 nm, however, the major size distribution was in the range of 15–20 nm (Figure 4b). The image clarifies that there is a shell core around the AgNPs, a core nanostructure that appears dark, in which nanocellulose appears as shells around the AgNPs. Capping of metal nanoparticles is one of the critical methods for ensuring its stability, AgNPs synthesized and capped by a secreted polysaccharide–protein matrix of *Spirulina platensis* were quasispherical shaped nanoparticles captured in a polysaccharide–protein matrix sheath with sizes ranging from 5.04 to 33.56 nm [66]. Rajeshkumar et al.'s [67] TEM results of AgNP-based chitosan nanocomposite found it to be spherical with a size of around 10–60 nm.

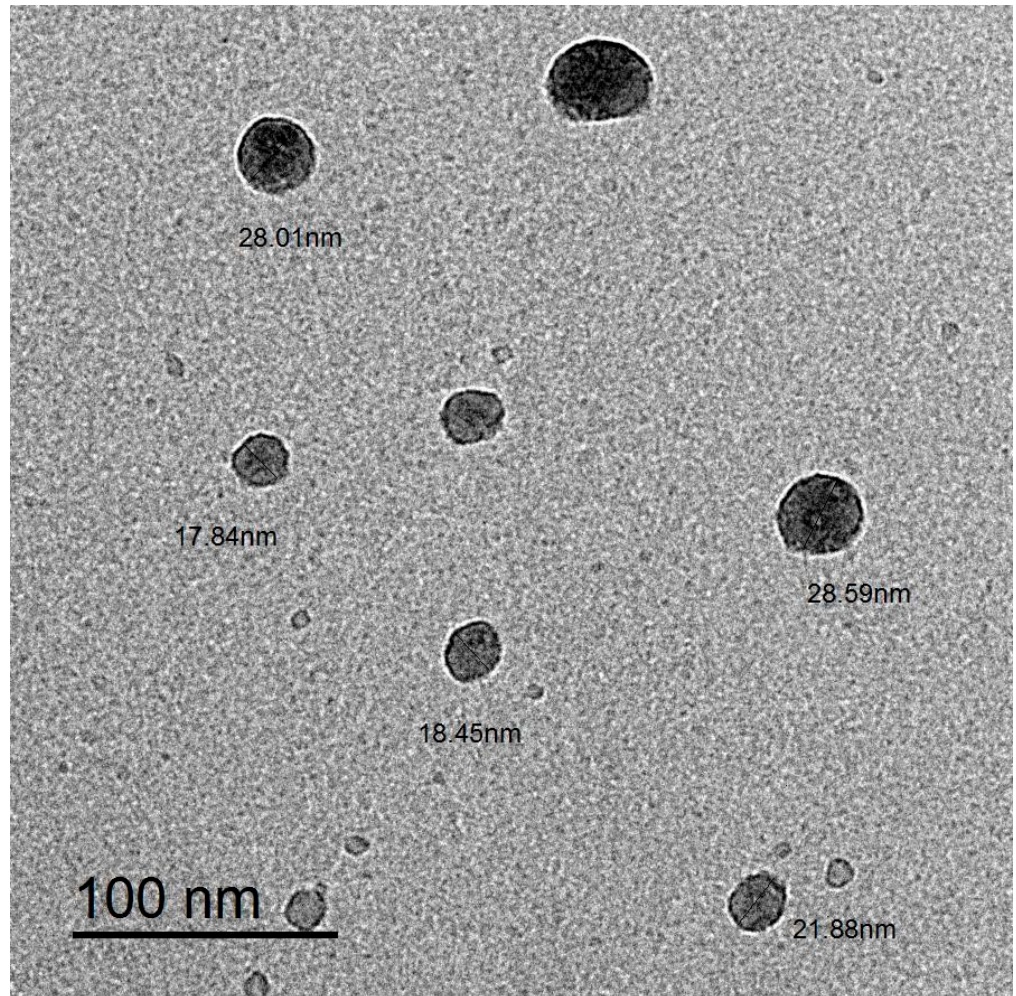


(a)



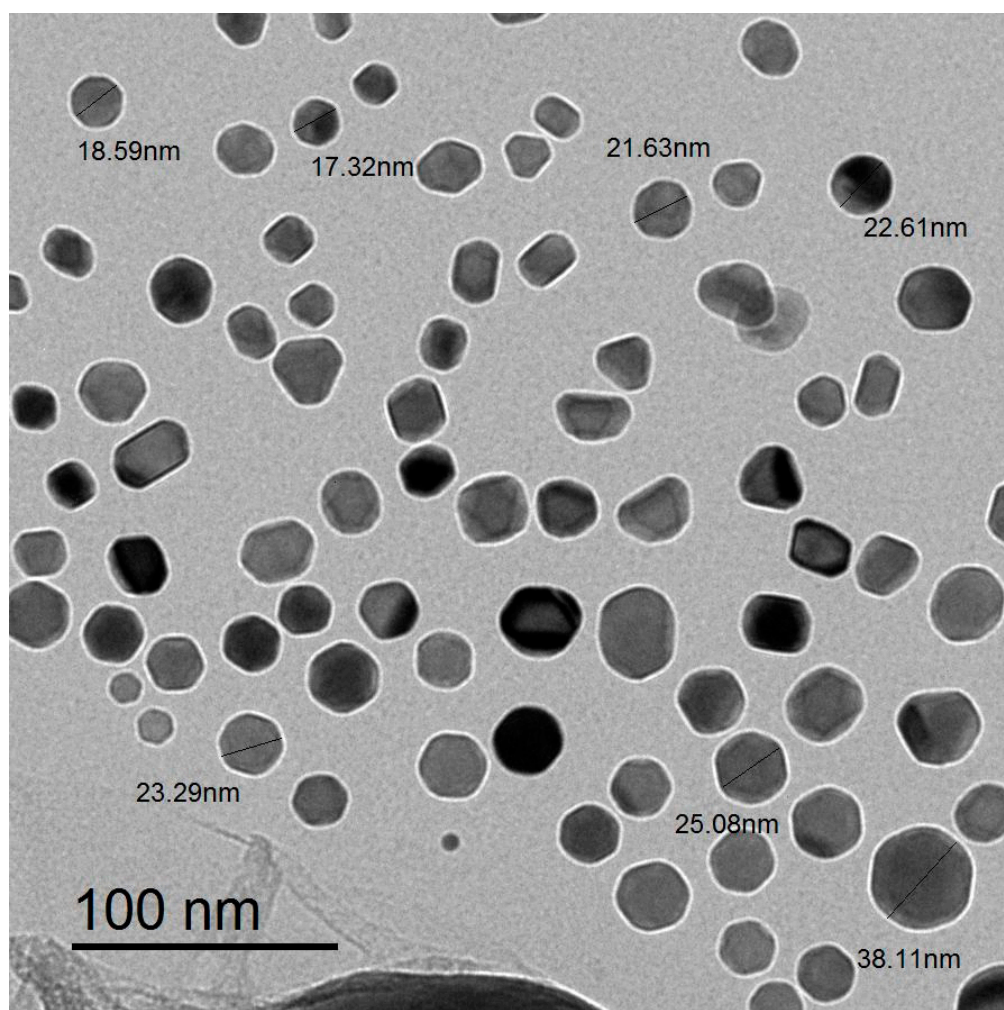
(b)

Figure 2. Scanning electron microscopic (SEM) image of biosynthesis: nanocellulose (a) and Ag/cellulose nanocomposites (b) derived from *U. lactuca*.



(a)

Figure 3. Cont.



(b)

Figure 3. Transmission electron microscopic (TEM) image of biosynthesis: Ulva/nanocellulose (a) and Ulva/Ag/cellulose nanocomposites (b).

3.3. Energy-Dispersive X-ray Measurements

An analytical method called energy-dispersive X-ray spectroscopy can be used to determine the relative abundance of different elements in a given sample. It depends on a sample and an X-ray excitation source interacting (Figure 5). EDS can be used to identify the chemical elements present in a sample and quantify their relative abundance (qualitative and quantitative analysis). The EDS analysis of nanocellulose derived from *U. lactuca* confirmed that there are nine elements, C, O, Al, Si, Cl, Ca, Fe, Cu, and Sb, with percentage weights of 41.3, 4.1, 0.29, 0.73, 5.85, 6.08, 0.45, 0.87, and 2.17, respectively. Also, there are nine elements presented in Ag/cellulose nanocomposites, C, O, Na, Mg, Cl, Ca, Fe, Rb, and Ag, with percentage weights of 25.86, 40.41, 2.41, 0.57, 11.59, 8.68, 0.88, 1.26, and 8.34%, respectively. The weight of carbon atoms, 41.3% in nanocellulose, became 25.86% in Ag/cellulose nanocomposites. It appears that Ag replaced carbon atoms in Ulva/nanocellulose and formed Ag/cellulose nanocomposites (Figure 4a,b). The analysis of the TiO₂/CNF composite using energy-dispersive X-ray spectroscopy (EDS) is mostly composed of the three elements, C, O, and Ti [68]. Energy-dispersive X-ray (EDX) analysis was used to emphasize the elemental structure of the silver nanospheres/graphene oxide composite [69]. Silver nanoparticles were well dispersed on the surface of cellulose and penetrated into the cellulose network [70].

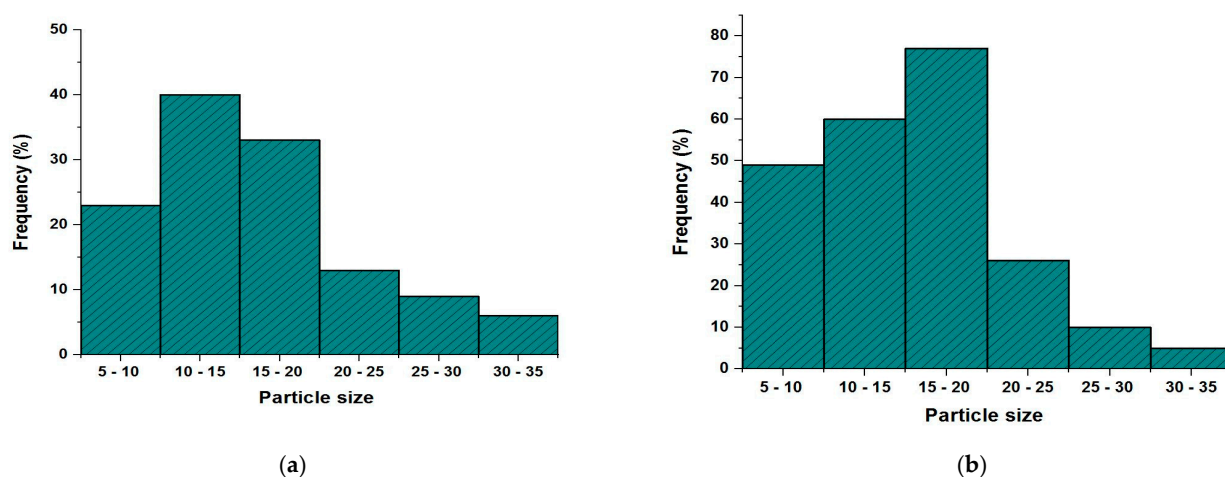
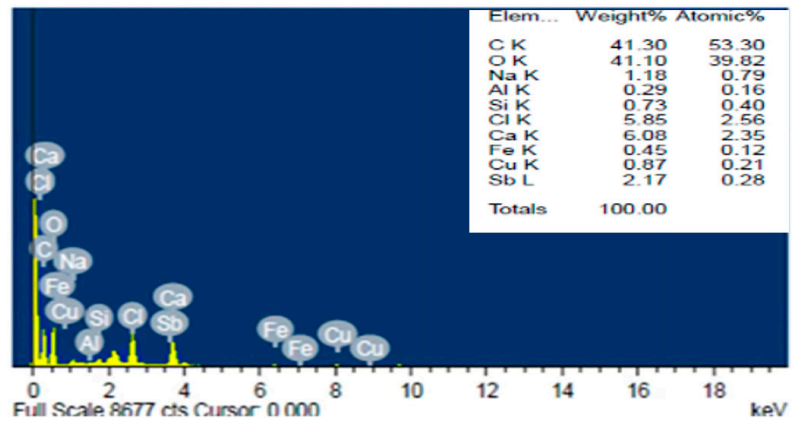


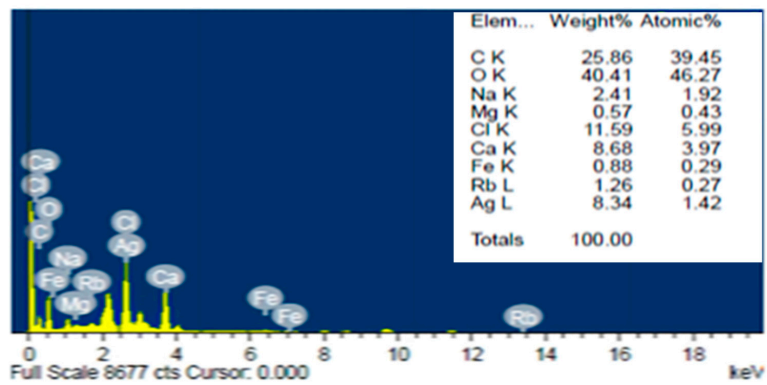
Figure 4. Particle size distribution of Ulva/nanocellulose (a) and Ulva/Ag/cellulose nanocomposites (b) derived from *U. lactuca*.

3.4. X-ray Diffraction

The intensity and shape of the peaks in the XRD patterns are affected by crystal size and crystalline shape. As can be seen, the XRD pattern of nanocellulose and Ulva/Ag/cellulose nanocomposites derived from *U. lactuca* indicate the crystal structure. The XRD diffraction patterns of nanocellulose derived from *U. lactuca* were recorded at 2θ , 10.8, 11.5, 15.1, 20.6, 21.9, 22.9, 25.4, 26.5, 27.9, 29, 31.6, 33.5, 34.6, 37.6, 40.4, 43.1, 45.5, 48.1, and 50.2, which correspond to lattice planes (hkl) (200), (210), (220), (400), (330), (331), (422), (431), (432), (440), (610), (443), (622), (551), (559), (733), (831), (911), and (762) (Figure 6a and Table 2). The major crystalline peak was obtained at 2θ (31.6°) with an intensity of 100% and crystalline size of 27.83, which confirmed that the nanocellulose obtained is nanocrystalline. The peaks at 2θ , 21.9, 22.9, and 45.5 are the broad bands and denote the amorphous nanocellulose. The conventional two-phase cellulose model illustrates cellulose chains as comprising both crystalline (ordered) and amorphous (less ordered) regions [71]. The methods of cellulose synthesis were affected in amorphous and crystalline regions in cellulose nanofibril (CNF) [22]. The XRD peaks of CNCs at 15° , 16.5° , 22.3° , and 34.4° reflect the (100), (110), (200), and (004) planes of cellulose [72]. The peaks of XRD diffraction patterns of Ulva/Ag/cellulose nanocomposites were recorded at 2θ , 20.6, 23.2, 27.7, 28.9, 29.5, 30.9, 31.6, 32.1, 36.2, 37.2, 43.3, 45.4, 47.5, 49.0, 54.6, 55.8, 56.4, 57.3, 58.2, 66.0, and 67.3 . The main crystalline peak was obtained at 2θ (32.1°) with an intensity of 100% and crystalline size of 31.35, and all peaks were sharp and all crystalline sizes in nm, which confirmed the crystalline Ulva/Ag/cellulose nanocomposites (Figure 6b and Table 2b). When the diffraction peak is quite sharp, which indicates that the silver has good crystallization performance [73]. The diffraction peaks at 38.1° , 44.19° , 64.4° , and 77.4° corresponding to lattice planes (hkl) from the (111), (200), (220), and (311) crystallographic planes of cubic AgNPs [74]. The XRD analysis of neat CNF-Ag NPs composites revealed the presence of Ag nanoparticles with the peaks at $2\theta = 37.68^\circ$, 43.97° , 64.12° and 77.22° which are corresponding to (111), (200), (220), and (311) in the region from 20 to 80° [75].

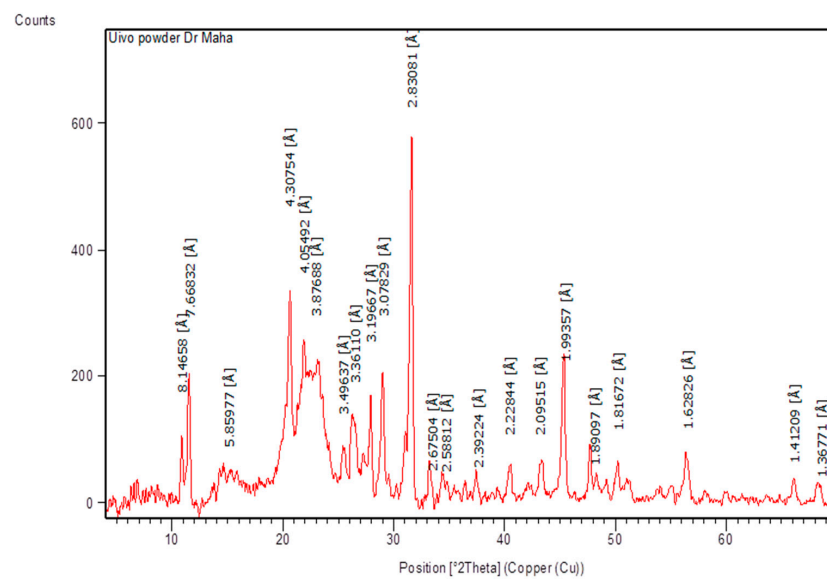


(a)



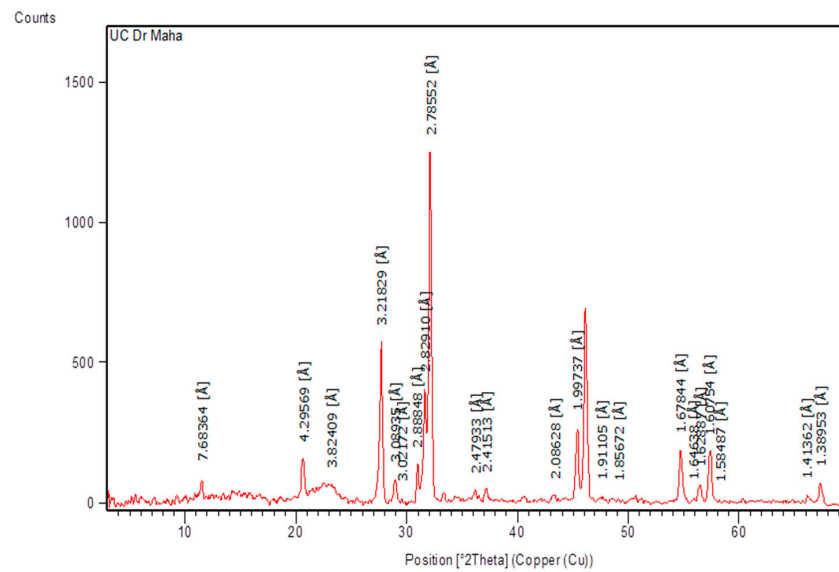
(b)

Figure 5. Energy-dispersive X-ray spectrophotometry analysis of biosynthesis: nanocellulose (a) and Ulva/Ag/cellulose nanocomposites (b) derived from *U. lactuca*.



(a)

Figure 6. Cont.



(b)

Figure 6. XRD analysis of biosynthesis: nanocellulose (a) and Ulva/Ag/cellulose nanocomposites (b) derived from *U. lactuca*.

Table 2. Simple peak indexing of Ulva/nanocellulose and Ulva/Ag/cellulose nanocomposites.) derived from *U. lactuca*.

S. No.	Peak Position 2θ	d-Spacing (Å)	hkl	Crystal Size L (nm)	Intensity %
1	10.8	8.14658	200	17.2683	27.72
2	11.5	7.66832	(210)	8342	41.83
3	15.1	5.85977	(220)	48	17.57
4	20.6	4.30754	(400)	26	62.3
5	21.9	4.05492	(330)	8454	49.84
6	22.9	3.87688	(331)	8464	41.9
7	25.4	3.49637	(422)	3.8	23.61
8	26.5	3.3611	(431)	10.17	29.41
9	27.9	3.19667	(432)	38.79	36.88
10	29	3.07829	(440)	28.07	41.9
11	31.6	2.83081	(610)	27.83	100
12	33.5	2.67504	(443)	96.32	13
13	34.6	2.58812	(622)	96.62	12.72
14	37.6	2.39224	(551)	97.43	13.66
15	40.4	2.22844	(559)	74.24	2.22844
16	43.1	2.09515	(733)	117	2.09515
17	45.5	1.99357	(831)	9001	1.99357
18	48.1	1.89097	(911)	101	1.89097
19	50.2	1.81672	(762)	35.6	1.81672

Table 2. Cont.

S. No.	Peak Position 2 θ	d-Spacing (Å)	hkl	Crystal Size L (nm)	Intensity %
1	11.5	7.68364	(000)	42.39	5.58
2	20.6	4.29569	(100)	35.72	10.51
3	23.2	3.82409	(110)	13.26	3.15
4	27.7	3.21829	(111)	28.96	45.55
5	28.9	3.08935	(111)	39.59	6.15
6	29.5	3.02172	(111)	72.69	0.95
7	30.9	2.88848	(111)	33.67	10.64
8	31.6	2.8291	(111)	73.84	32.05
9	32.1	2.78552	(111)	31.35	100
10	36.2	2.47933	(200)	49.32	2.42
11	37.2	2.41513	(210)	44.51	2.83
12	43.3	2.08628	(211)	25.22	1.3
13	45.4	1.99737	(211)	30.48	20.18
14	47.5	1.91105	(211)	19.21	1
15	49.0	1.85672	(220)	77.26	0.87
16	54.6	1.67844	(310)	27.93	14.53
17	55.8	1.64638	(310)	47.74	1.01
18	56.4	1.62887	(310)	29.93	4.54
19	57.3	1.60754	(310)	32.05	13.84
20	58.2	1.58487	(311)	60.36	0.6
21	66.0	1.41362	(320)	55.92	1.66
22	67.3	1.38953	(321)	41.65	5.48

3.5. Zeta Potential Analysis

From the zeta potential results presented in Figure 7a,b, it is noticeable that the surface charge of the nanocellulose derived from *U. lactuca* has a negative charge of -0.217 mV, and Ulva/Ag cellulose nanocomposite is -16.4 mV. The results demonstrate that Ulva/Ag cellulose nanocomposites are more negative than Ulva/nanocellulose. Abo-Elmagd et al. [76] stated that charges and strong resistive forces between the particles prevent aggregation and keep the nanoparticles in the medium stable. The zeta potential value of AgNPs photo-synthesized by *Oscillatoria limnetica* was -27.4 [77]. The negative charge of nanoparticles revealed the repulsion among the nanoparticles and superior constancy. In agreement with this study, the Au/cellulose nanocomposite biofabricated by green alga *Chlorella vulgaris* is negative (-13.6 mV) [78]. The difference in zeta potential values of these results and other research may be due to the zeta potential of cellulose nanocrystal (CNC) aqueous dispersions, as was the function of solution conditions, including changing pH and different electrolyte identities and concentrations [79].

3.6. Differential Scanning Calorimetry (DSC)

Figure 8 displays the DSC thermogram of Ulva/Ag/cellulose nanocomposites blended with fluoride, the temperature ranged from 20 °C to 600 °C. The glass transition temperature (T_g) 117.237 °C, was attained. The exothermic exhibited in the range of 148.648 and 169.788 °C may be due to the result of water evaporation. Composites exhibited initial decomposition around 100 °C, which could be due to the result of water evaporation [80]. According to the DSC curve, drug dehydration occurred between 50 and 121.8 °C [81].

In the second exothermic peak, ranging from 225 and 317.12 °C, thermal decomposition of cellulose nanocomposites was exhibited. The results are in agreement with Peter and Chrebet's [82] reported cellulose decomposition beginning at temperatures of 250–260 °C. The results demonstrated the presence of exothermic peak during the heating scan of differential scanning calorimeter (DSC) analysis, called the cold crystallization peaks [83].

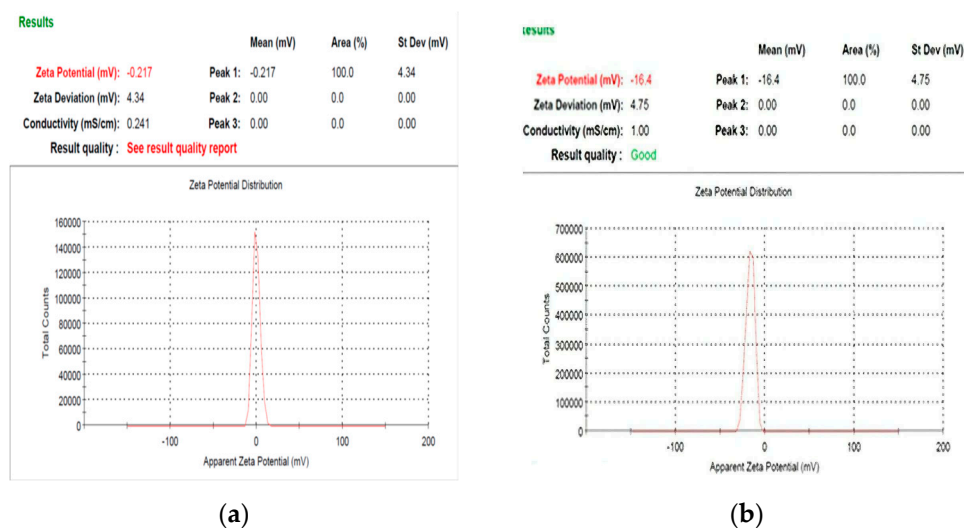


Figure 7. Zeta potential analysis of biosynthesis: nanocellulose (a) and Ulva/Ag/cellulose nanocomposites (b) derived from *U. lactuca*.

3.7. Antimicrobial Activity

The agar-well diffusion technique was used to investigate the antibacterial activities of hybrids made of AgNPs, Ulva/nanocellulose, and Ulva/Ag/cellulose nanocomposite at different concentrations of nanocellulose (0.1, 0.2, 0.4, and 0.8 g) against both *S. mutans* ATCC 25175 and *L. acidophilus* CH-2.

Results obtained from the clear zone (mm) around the two bacterial types revealed that all examined nanoparticles have antibacterial activity on selected indicator organisms, however, Ulva/nanocellulose showed low antibacterial activity. Both AgNPs and Ulva/Ag/cellulose nanocomposite showed greater inhibitory zone diameter than that obtained by Ulva/nanocellulose. Furthermore, no significant differences in inhibition zone diameter were observed when different cellulose concentrations were applied to process Ulva/Ag/cellulose nanocomposites (Figure 9 and Table 3). The interaction and toxicity of nanoparticles are more significant with the bacterial surface due to their small size and high surface area. [23]. Results in Figure 8 and Table 3 demonstrate Ulva/nanocellulose possessed low antibacterial activities against both *S. mutans* ATCC 25175 and *L. acidophilus* CH-. Nanocellulose, by nature, does not have any antimicrobial properties and needs surface modification to make it an antimicrobial material [84]. Khulbe and Matsuura [85] recorded metal/metal oxide nanoparticles (such as Cu, Au, CuO, ZnO, Ag, TiO₂, and MgO), silanes, chlorine, and chitosan as coupling agents that provide nanocellulose with antimicrobial properties. In a previous study, nanocellulose was modified by combining it with chitosan to inhibit the growth of *Escherichia coli* by 99% [86]. Oxide/cellulose nanocomposite presented afflicted antibacterial activity against *Staphylococcus aureus* and *E. coli* [27]. The AgNPs cellulose composite showed excellent antibacterial activity to prohibit bacterial infection and biofilm formation efficacy against most types of bacteria [87]. These nanoparticles have different mechanisms of action, including damaging the bacterial cell membrane by transference of Ag⁰ to Ag⁺, as well as the obstruction of the intercellular metabolic pathways following Ag⁺ penetration into the cell [88]. Antibacterial experimental results showed that the cellulose–silver hybrids showed excellent antimicrobial activities against *E. coli* (Gram-negative) and *S. aureus* (Gram-positive) [70]. Since they exhibit antibacterial properties, CNF/ZnO films can be utilized in biological applications [89]. The

antibacterial activity of silver against *K. pneumonia* strains (Gram-negative bacteria) and *S. aureus* (Gram-positive bacteria) has been reported [90]. Silver ions change the function of the bacterial wall after binding with it [91]. El-Abd et al. [92] reported that coating biosynthesis AgNPs with acetic acid reduced the microflora in Ross broiler chicks such as *Pseudomonas orizihabitain*. Hamouda et al. [93] estimated that biosynthesis AgNPs using two red algae capping SDS possessed antibacterial activities against *Micrococcus leutus*, *Kocuria varians*, and *Escherichia coli* ATCC 8739. Silver nanoparticles biofabricated by *Oscillatoria limnetica* demonstrated the highest antibacterial activity against multidrug-resistant bacteria (MDR) [77].

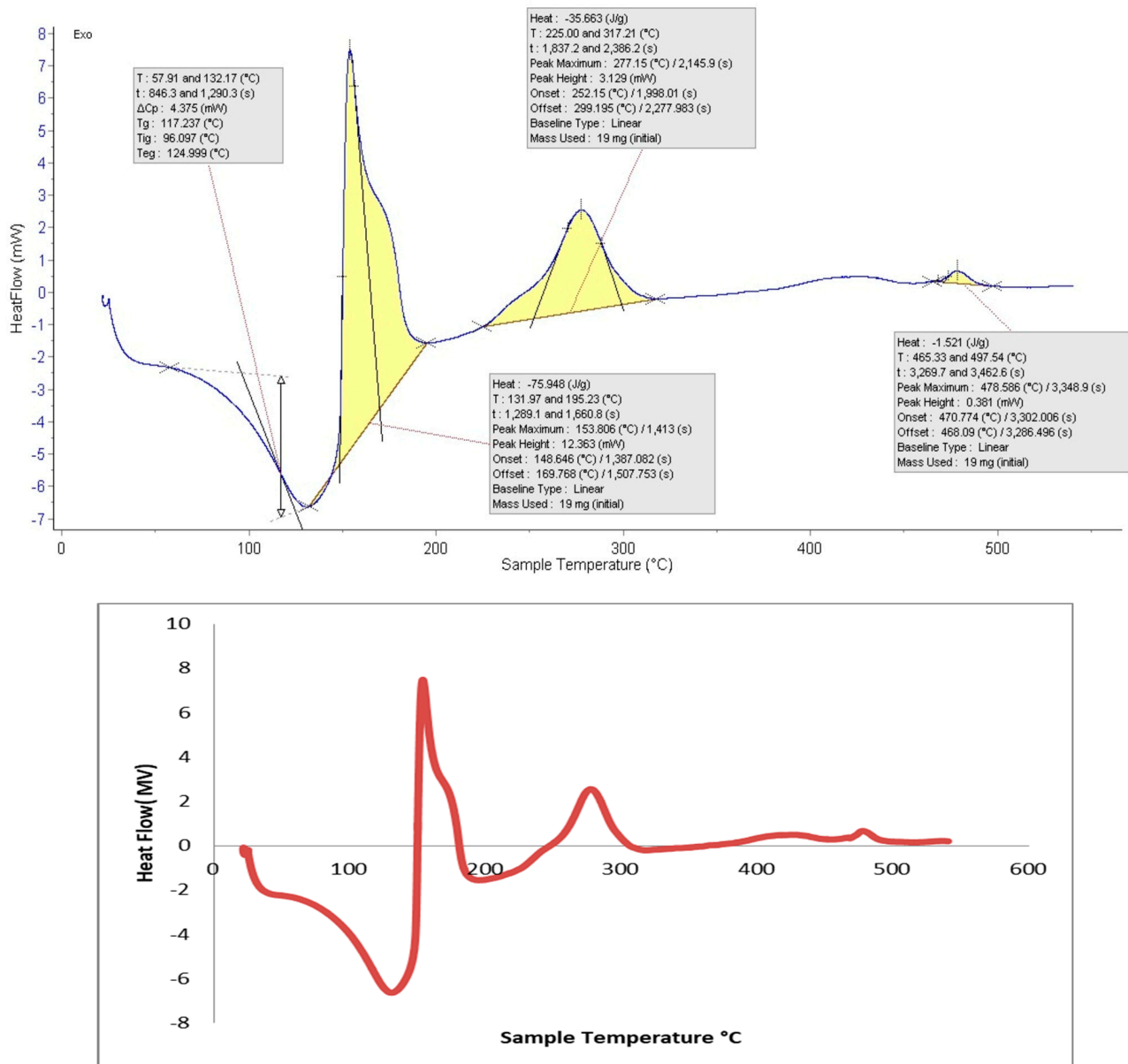


Figure 8. DSC of Ulva/Ag/cellulose nanocomposite blend with fluoride.

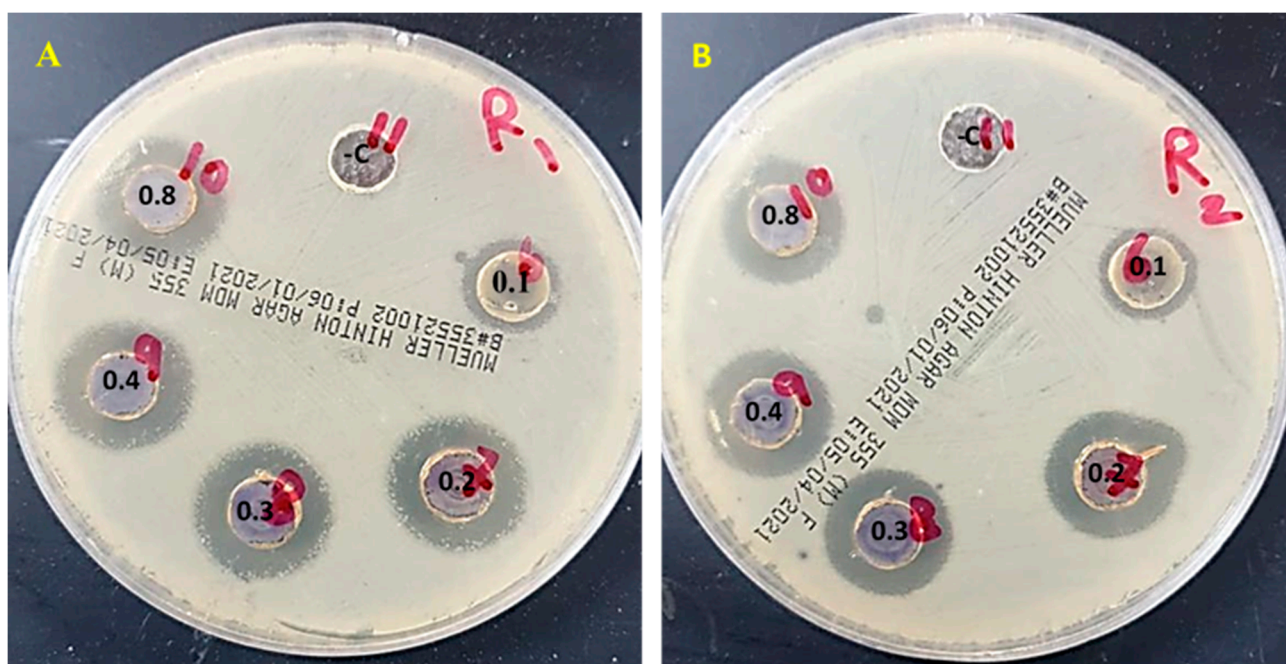


Figure 9. Antimicrobial activity of control, Ulva/nanocellulose, and Ulva/Ag/cellulose nanocomposite at different concentrations of cellulose (0.1, 0.2, 0.4, and 0.8 g) against both (A) *S. mutans* ATCC 25175 (R1) and (B) *L. acidophilus* CH-2 (R2). Clear zones (11), control Ulva extract, (6) Ulva/nanocellulose, clear zone of different cellulose concentrations (0.1, 0.2, 0.4, and 0.8 g) of Ulva/Ag/cellulose nanocomposite (7, 8, 9, and 10), respectively.

Table 3. Inhibition zone diameter (mm) of *S. mutans* ATCC 25175 and *L. acidophilus* CH-2 at different concentrations of cellulose percentage to form Ulva/Ag/cellulose nanocomposites, Ulva/AgNPs, and nanocellulose derived from *U. lactuca*.

Strains	B	A	(C) with Cellulose Conc., %				Control
			1.6	0.8	0.4	0.2	
<i>S. mutans</i>	18 ± 0.2 c	18 ± 0.1 c	18 ± 0.2 c	19 ± 0.1 c	16 ± 0.00 b	13 ± 0.2 a	0
<i>L. acidophilus</i>	17 ± 0.13 c	18 ± 0.1 c	18 ± 0.05 c	18 ± 0.05 c	15 ± 0.1 b	13 ± 0.1 a	0

Nanocellulose 4 mg/mL (A); Ulva/AgNPs, 1.7 mg/mL (B); Ulva/Ag/cellulose nanocomposites (C). Different letters denote significance value at $p < 0.05$. Control: Ulva water extract.

3.8. Antimicrobial Activity of Nanocellulose Blended with Fluoride

The results presented in Table 4 show that fluoride had no inhibition zone present with two bacterial strains, while nanocellulose blended with fluoride was more effective than nanocellulose and Ulva/Ag/cellulose nanocomposites/fluoride in the case of *S. mutans* ATCC 25175. Ulva/Ag/cellulose nanocomposites/fluoride possessed more activity than nanocellulose/fluoride against *L. acidophilus* CH-2. Fluoridated polyethylene glycol-coated silver nanoparticles (PEG-AgNPs) can be used for antibacterial activity against *S. mutans* [94]. Silver nanoparticles blended with fluoride had antibacterial activity against *Streptococcus mutans* [95]. In comparison with sodium fluoride, silver nanofluoride was more effective in inhibiting pH lowering and adherence of *S. mutans* to the enamel surface [96]. Widakdo et al. [97] reported graphene oxide (GO) had antibacterial qualities against *Escherichia coli*, and the antibacterial level increased to 99.9% in almost all membranes with different pH values, due to the synergistic effect between AgNPs, GO, GO-Ag-pHx that showed a lower molecular transmission resistance and a higher antibacterial effect. Linear low-density polyethylene (LLDPE) combined with CaO and metal

ion forms (LLDPE/CaO Ag, LLDPE/CaO Zn, and LLDPE/CaO Cu) were excellent and functioned as antibacterial agents against *E. coli* with an antibacterial rate of 99.9% [98].

Table 4. Inhibition zone diameter (mm) of *S. mutans* ATCC 25175 and *L. acidophilus* CH-2 of Ulva/cellulose and Ulva/Ag/cellulose nanocomposites that were blended with fluoride. (Different letters denote significance value $p < 0.05$).

Bacterial Strain	Nanocellulose	Ulva/AgNPs	Fluoride	Nanocellulose/Fluoride	Ulva/Ag/Cellulose Nanocomposites/Fluoride
<i>S. mutans</i>	13 ± 0.2 a	16 ± 0.00 b	0	23 ± 2 c	22 ± 1 c
<i>L. acidophilus</i>	13 ± 0.2 a	15 ± 0.1 b	0	23 ± 1 c	24 ± 2 c

3.9. Minimum Inhibitory Concentration (MIC)

The MIC values of Ulva/Ag/cellulose nanocomposites were tested against *S. mutans* ATCC 25175 and *L. acidophilus* CH-2 at concentrations ranging from 0.0018 to 0.000056 g/mL. The inhibition zone diameter values (mm) were dose dependent and gradually decreased by decreasing the concentration of Ag/Ulva/cellulose nanocomposites (Table 5 and Figure 10). The results show that the MIC of both bacteria was 0.000112 g/mL (0.112 mg/L). Hamouda et al. [92] reported that the MIC of AgNPs synthesis by marine green alga *Ulva fasciata* is 0.5 mg/mL for *S. aureus*, 1.0 mg/mL for *Salmonella enterica* sub sp., 0.5 mg/mL for *Aeromonas hydrophila*, 2 mg/mL for *E. coli* O157, and 1.0 mg/mL for *Bacillus cereus*. There are many studies that have proved the antibacterial activities of AgNPs derived from biomaterials and Ag cellulose nanocomposites against different bacteria, as tabulated in Table 6.

Table 5. Inhibition zone (mm) of *S. mutans* ATCC 25175 and *L. acidophilus* CH-2 at different concentrations of Ag/Ulva cellulose nanocomposites (g/mL) after 24 h.

Nanocomposites (g/mL)	0.0018	0.0009	0.00045	0.000225	0.000112	0.000056
<i>S. mutans</i>	19 ± 0.1	18 ± 0.3	15 ± 0.1	14 ± 0.00	11 ± 0.00	0 ±
<i>L. acidophilus</i>	19 ± 0.00	18 ± 0.1	15 ± 0.1	13 ± 0.00	12 ± 0.00	0 ±

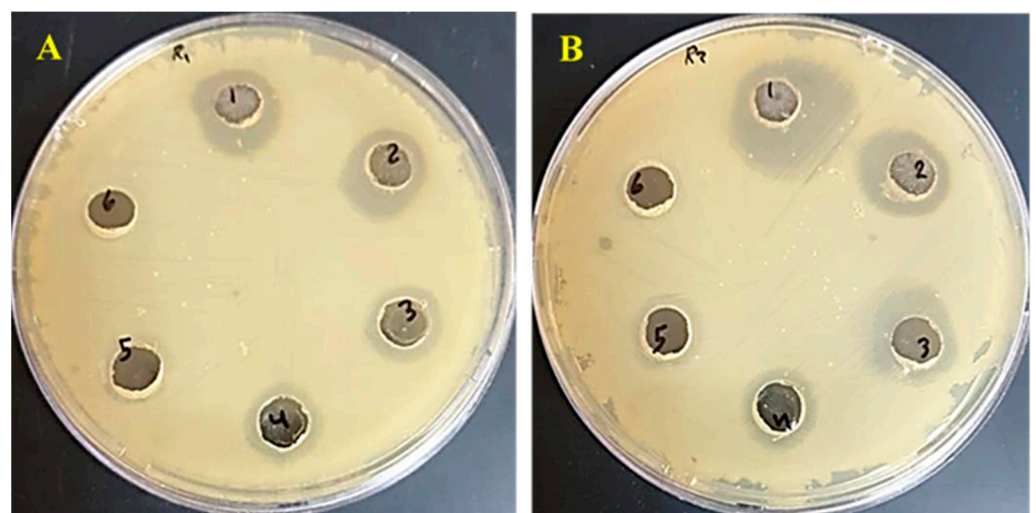


Figure 10. Effect of different concentrations (mg/mL) of Ulva /Ag/cellulose nanocomposites on *S. mutans* (A) and *L. acidophilus* (B).

Table 6. Comparison study with other researches on antibacterial activity.

	Sources	Antibacterial Against	Reference
AgNPs	<i>Sargassum wightii</i>	<i>Micrococcus luteus</i> , <i>Serratia marcescens</i>	[99]
	<i>Caulerpa serrulata</i>	<i>E. coli</i> , <i>Salmonella typhi</i>	[100]
	<i>Caulerpa racemosa</i>	<i>Staphylococcus aureus</i> , <i>Proteus mirabilis</i>	[101]
	<i>Chlorella ellipsoidea</i> .	<i>S. aureus</i> , <i>P. aeruginosa</i> , <i>K. pneumonia</i> , <i>E. coli</i>	[102]
	<i>Ecklonia cava</i>	<i>E. coli</i>	[103]
AgNPS/Cellulose	Orange peel waste	<i>E. coli</i>	[104]
	Cotton pulp cellulose	<i>E. coli</i> , <i>P. aeruginosa</i> , <i>S. aureus</i>	[105]
	Bacterial cellulose	<i>B. subtilis</i> , <i>S. aureus</i> , <i>E. coli</i>	[106]
	Bacterial cellulose	<i>Escherichia coli</i> <i>Staphylococcus aureus</i>	[107]
	Ag/ <i>Ulva</i> cellulose nanocomposites	<i>S. mutans</i> ATCC 25175 and <i>L. acidophilus</i> CH-2	This study

4. Conclusions

Nanocomposites have led to hurriedly increasing applications in various fields. This study investigated the effect of nanocellulose and *Ulva*/Ag/cellulose nanocomposites derived from marine alga *Ulva lactuca* against *S. mutans* ATCC 25175 and *L. acidophilus* CH-2. *Ulva*/nanocellulose and *Ulva*/Ag/cellulose nanocomposites were characterized by TEM, SEM, zeta potential, EDX, XRD, and FT-IR. SEM confirmed that nanocellulose comprises filaments, and *Ulva*/Ag cellulose nanocomposites have fibrous surfaces. TEM images showed that the diameter of *Ulva*/nanocellulose ranged from 17 to 28 nm, while the diameter size of *Ulva*/Ag cellulose nanocomposites was 18.59 to 38.11. XRD confirmed that both *Ulva*/nanocellulose and *Ulva*/Ag cellulose nanocomposites were crystalline. Zeta potential indicated that *Ulva*/Ag cellulose nanocomposites were more negative in charge than *Ulva*/nanocellulose. *Ulva*/nanocellulose and *Ulva*/Ag cellulose nanocomposites have antibacterial activity against *S. mutans* and *L. acidophilus*. Data analysis revealed that *Ulva*/Ag/cellulose nanocomposites are more effective than *Ulva*/nanocellulose, and *Ulva*/Ag/cellulose nanocomposites blended with fluoride had more antibacterial activity than those not blended with fluoride. The antibacterial activities showed nonsignificant differences based on using different cellulose concentrations. Based on the data obtained, it is possible to deduce that *Ulva*/Ag/cellulose nanocomposites have the potential to be an economical and safe nanocomposite product from a natural source with antibacterial components that might be employed against bacteria that cause dental decay, blended to toothpaste, and add to tooth filler.

Author Contributions: R.A.H. conceptualization, data analysis, validation, supervision and writing. F.A.K.Q., methodology, and writing. F.S.S. and T.M.A.-S., investigation and resources. R.R.M., methodology, supervision. All authors have read and agreed to the published version of the manuscript.

Funding: This research received no external funding.

Institutional Review Board Statement: Not applicable.

Informed Consent Statement: Not applicable.

Data Availability Statement: The datasets spent and/or analyzed during this study are available from the corresponding author upon reasonable request.

Conflicts of Interest: The authors declare no conflict of interest.

References

1. Uerlich, M.F.; Baker, S.R.; Day, P.F.; Brown, L.; Vettore, M.V. Common Determinants of Dental Caries and Obesity in Children: A Multi-Ethnic Nested Birth Cohort Study in the United Kingdom. *Int. J. Environ. Res. Public Health* **2021**, *18*, 12561. [CrossRef]
2. Seymour, B.; James, Z.; Shroff Karhade, D.; Barrow, J.; Pruneddu, A.; Anderson, N.K.; Definition of Global Health, T.F.F.T. A definition of global oral health: An expert consensus approach by the Consortium of Universities for Global Health's Global Oral Health Interest Group. *Glob. Health Action* **2020**, *13*, 1814001. [CrossRef]
3. Veiga, N.; Pereira, C.; Amaral, O. Prevalence and determinants of dental caries in Portuguese children. *Procedia-Soc. Behav. Sci.* **2015**, *171*, 995–1002. [CrossRef]
4. Selwitz, R.H.; Ismail, A.I.; Pitts, N.B. Dental caries. *Lancet* **2007**, *369*, 51–59. [CrossRef]
5. Featherstone, J.D. Dental caries: A dynamic disease process. *Aust. Dent. J.* **2008**, *53*, 286–291. [CrossRef]
6. Rostinawati, T.; Aryani, H.; Iskandar, Y. Identification of bacteria causing dental caries through genetic testing and activity assay of toothpastes. *J. Pharm. Sci. Res.* **2018**, *10*, 511–513.
7. Mitchell, T.J. The pathogenesis of streptococcal infections: From tooth decay to meningitis. *Nat. Rev. Microbiol.* **2003**, *1*, 219–230. [CrossRef]
8. Yadav, K.; Prakash, S. Dental caries: A microbiological approach. *J. Clin. Infect. Dis. Pract.* **2017**, *2*, 1–15. [CrossRef]
9. Hohwy, J.; Reinholdt, J.; Kilian, M. Population dynamics of *Streptococcus mitis* in its natural habitat. *Infect. Immun.* **2001**, *69*, 6055–6063. [CrossRef]
10. Kulshrestha, A.; Gupta, P. Polymicrobial interaction in biofilm: Mechanistic insights. *Pathog. Dis.* **2022**, *80*, ftac010. [CrossRef]
11. Loesche, W.J. Microbiology of Dental Decay and Periodontal Disease. In *Medical Microbiology*, 4th ed.; University of Texas Medical Branch at Galveston: Galveston, TX, USA, 1996; Chapter 99. Available online: <https://www.ncbi.nlm.nih.gov/books/NBK8259/> (accessed on 10 October 2022).
12. Desselberger, U. Emerging and re-emerging infectious diseases. *J. Infect.* **2000**, *40*, 3–15. [CrossRef] [PubMed]
13. Abiodun Solanke, I.M.F.; Ajayi, D.M.; Arigbede, A.O. Nanotechnology and its application in dentistry. *Ann. Med. Health Sci. Res.* **2014**, *4*, 171–177. [CrossRef] [PubMed]
14. De Kwaadsteniet, M.I.C.H.E.L.E.; Botes, M.; Cloete, T.E. Application of nanotechnology in antimicrobial coatings in the water industry. *Nano* **2011**, *6*, 395–407. [CrossRef]
15. Bhutiya, P.L.; Misra, N.; Rasheed, M.A.; Hasan, S.Z. Silver Nanoparticles Deposited Algal Nanofibrous Cellulose Sheet for Antibacterial Activity. *BioNanoScience* **2020**, *10*, 23–33. [CrossRef]
16. Moon, R.J.; Martini, A.; Nairn, J.; Simonsen, J.; Youngblood, J. Cellulose nanomaterials review: Structure, properties and nanocomposites. *Chem. Soc. Rev.* **2011**, *40*, 3941–3994. [CrossRef] [PubMed]
17. Al-Jawhari, I.F.H. Nanocellulose for Sustainable Future Applications. In *Handbook of Nanomaterials and Nanocomposites for Energy and Environmental Applications*; Springer: Berlin/Heidelberg, Germany, 2020; pp. 1–12. [CrossRef]
18. Naz, S.; Ali, J.S.; Zia, M. Nanocellulose isolation characterization and applications: A journey from non-remedial to biomedical claims. *Bio-Des. Manuf.* **2019**, *2*, 187–212. [CrossRef]
19. Saleh, M.H.S.D.E.; Muhamad, M.D.I.L.; Mamat, S.N.H. Cellulose Nanofiber Isolation and Its Fabrication into Bio-Polymer-A Review. In Proceedings of the International Conference on Agricultural and Food Engineering for Life (Cafei2012), Putrajaya, Malaysia, 26–28 November 2012; Volume 26, p. 28.
20. Iwamoto, S.; Kai, W.; Isogai, A.; Iwata, T. Elastic modulus of single cellulose microfibrils from tunicate measured by atomic force microscopy. *Biomacromolecules* **2009**, *10*, 2571–2576. [CrossRef]
21. Klemm, D.; Kramer, F.; Moritz, S.; Lindström, T.; Ankerfors, M.; Gray, D.; Dorris, A. Nanocelluloses: A new family of nature-based materials. *Angew. Chem. Int. Ed.* **2011**, *50*, 5438–5466. [CrossRef]
22. Beck, S.; Bouchard, J.; Berry, R. Controlling the reflection wavelength of iridescent solid films of nanocrystalline cellulose. *Biomacromolecules* **2011**, *12*, 167–172. [CrossRef]
23. Lee, K.Y.; Aitomäki, Y.; Berglund, L.A.; Oksman, K.; Bismarck, A. On the use of nanocellulose as reinforcement in polymer matrix composites. *Compos. Sci. Technol.* **2014**, *105*, 15–27. [CrossRef]
24. Jorfi, M.; Foster, E.J. Recent advances in nanocellulose for biomedical applications. *J. Appl. Polym. Sci.* **2015**, *132*. [CrossRef]
25. Liu, A.; Walther, A.; Ikkala, O.; Belova, L.; Berglund, L.A. Clay nanopaper with tough cellulose nanofiber matrix for fire retardancy and gas barrier functions. *Biomacromolecules* **2011**, *12*, 633–641. [CrossRef]
26. Lefatshe, K.; Muiva, C.M.; Kebaabetswe, L.P. Extraction of nanocellulose and in-situ casting of ZnO/cellulose nanocomposite with enhanced photocatalytic and antibacterial activity. *Carbohydr. Polym.* **2017**, *164*, 301–308. [CrossRef]
27. Janpetch, N.; Saito, N.; Rujiravanit, R. Fabrication of bacterial cellulose-ZnO composite via solution plasma process for antibacterial applications. *Carbohydr. Polym.* **2016**, *148*, 335–344. [CrossRef]
28. Dong, Y.Y.; Liu, S.; Liu, Y.J.; Meng, L.Y.; Ma, M.G. Ag@Fe₃O₄@cellulose nanocrystals nanocomposites: Microwave-assisted hydrothermal synthesis, antimicrobial properties, and good adsorption of dye solution. *J. Mater. Sci.* **2017**, *52*, 8219–8230. [CrossRef]
29. Xiong, R.; Lu, C.; Wang, Y.; Zhou, Z.; Zhang, X. Nanofibrillated cellulose as the support and reductant for the facile synthesis of Fe₃O₄/Ag nanocomposites with catalytic and antibacterial activity. *J. Mater. Chem. A* **2013**, *1*, 14910–14918. [CrossRef]
30. Dong, Y.Y.; Deng, F.; Zhao, J.J.; He, J.; Ma, M.G.; Xu, F.; Sun, R.C. Environmentally friendly ultrasound synthesis and antibacterial activity of cellulose/Ag/AgCl hybrids. *Carbohydr. Polym.* **2014**, *99*, 166–172. [CrossRef]

31. Leverett, D.H. Fluorides and the changing prevalence of dental caries. *Science* **1982**, *217*, 26–30. [[CrossRef](#)]
32. Featherstone, J.D. Prevention and reversal of dental caries: Role of low level fluoride. *Community Dent. Oral Epidemiol.* **1999**, *27*, 31–40. [[CrossRef](#)]
33. Whelton, H.P.; Spencer, A.J.; Do, L.G.; Rugg-Gunn, A.J. Fluoride revolution and dental caries: Evolution of policies for global use. *J. Dent. Res.* **2019**, *98*, 837–846. [[CrossRef](#)]
34. Palmer, J.D. Dental health in children—An improving picture? *Br. Dent. J.* **1980**, *149*, 48–50. [[CrossRef](#)]
35. Pitts, N.B.; Zero, D.T.; Marsh, P.D.; Ekstrand, K.; Weintraub, J.A.; Ramos-Gomez, F.; Ismail, A. Dental caries. *Nat. Rev. Dis. Prim.* **2017**, *3*, 17030. [[CrossRef](#)]
36. Arends, J.; Christoffersen, J. Nature and role of loosely bound fluoride in dental caries. *J. Dent. Res.* **1990**, *69* (Suppl. S2), 601–605. [[CrossRef](#)]
37. Cury, J.A.; Tenuta, L.M.A.; Ribeiro, C.C.C.; Paes Leme, A.F. The importance of fluoride dentifrices to the current dental caries prevalence in Brazil. *Braz. Dent. J.* **2004**, *15*, 167–174. [[CrossRef](#)]
38. Elgamily, H.; Safy, R.; Makharita, R. Influence of Medicinal Plant Extracts on the Growth of Oral Pathogens Streptococcus Mutans and Lactobacillus Acidophilus: An In-Vitro Study. *Open Access. Maced. J. Med. Sci.* **2019**, *7*, 2328. [[CrossRef](#)]
39. Chen, X.; Zou, L.Q.; Niu, J.; Liu, W.; Peng, S.F.; Liu, C.M. The stability, sustained release and cellular antioxidant activity of curcumin nanoliposomes. *Molecules* **2015**, *20*, 14293–14311. [[CrossRef](#)]
40. Greve, C.; Preketes, N.K.; Costard, R.; Koeppe, B.; Fidder, H.; Nibbering, E.T.J.; Temps, F.; Mukamel, S.; Elsaesser, T. N–H stretching modes of adenine monomer in solution studied by ultrafast nonlinear infrared spectroscopy and ab initio calculations. *J. Phys. Chem. A* **2012**, *116*, 7636–7644. [[CrossRef](#)]
41. Marchewka, M.K. Infrared and Raman spectra of bis (melaminium) sulfate dihydrate. *J. Chem. Res.* **2003**, *8*, 518–521. [[CrossRef](#)]
42. Stone, N.; Kendall, C.; Smith, J.; Crow, P.; Barr, H. Raman spectroscopy for identification of epithelial cancers. *Faraday Discuss.* **2004**, *126*, 141–157. [[CrossRef](#)]
43. Choo, L.P.; Mansfield, J.R.; Pizzi, N.; Somorjai, R.L.; Jackson, M.; Halliday, W.C.; Mantsch, H.H. Infrared spectra of human central nervous system tissue: Diagnosis of alzheimer’s disease by multivariate analyses. *Biospectroscopy* **1995**, *1*, 141–148. [[CrossRef](#)]
44. Wang, Y.; Zhou, Q.; Li, B.; Liu, B.; Wu, G.; Ibrahim, M.; Xie, G.; Li, H.; Sun, G. Differentiation in MALDI-TOF MS and FTIR spectra between two closely related species *Acidovorax oryzae* and *Acidovorax citrulli*. *BMC Microbiol.* **2012**, *12*, 182. [[CrossRef](#)] [[PubMed](#)]
45. Stenstad, P.; Andresen, M.; Tanem, B.S.; Stenius, P. Chemical surface modifications of microfibrillated cellulose. *Cellulose* **2008**, *15*, 35–45. [[CrossRef](#)]
46. Pramono, E.; Utomo, S.B.; Wulandari, V.; Clegg, F. FTIR studies on the effect of concentration of polyethylene glycol on polymerization of Shellac. *J. Phys. Conf. Ser.* **2016**, *776*, 012053.
47. Brown, M.D.; Hart, C.; Gazi, E.; Gardner, P.; Lockyer, N.; Clarke, N. Influence of omega-6 PUFA arachidonic acid and bone marrow adipocytes on metastatic spread from prostate cancer. *Br. J. Cancer* **2010**, *102*, 403–413. [[CrossRef](#)]
48. Wang, X.; Qi, Z.; Wang, S.; Liu, G.; Gao, H.; Tian, Y. The study of a single BGC823 cell using Fourier transform infrared microspectroscopic imaging. *Spectrochim. Acta Part A Mol. Biomol. Spectrosc.* **2011**, *79*, 1660–1662. [[CrossRef](#)]
49. Verdonck, M.; Denayer, A.; Delvaux, B.; Garaud, S.; De Wind, R.; Desmedt, C.; Sotiriou, C.; Willard-Gallo, K.; Goormaghtigh, E. Characterization of human breast cancer tissues by infrared imaging. *Analyst* **2016**, *141*, 606–619. [[CrossRef](#)]
50. Pandey, A.; Jariwala, K.N. Detection of adulteration in ghee from markets of Ahmedabad by FT-IR spectroscopy. *J. Chem. Pharm. Res.* **2015**, *7*, 10–14.
51. Junhom, C.; Weerapreeyakul, N.; Tanthanuch, W.; Thumanu, K. FTIR microspectroscopy defines early drug resistant human hepatocellular carcinoma (HepG2) cells. *Exp. Cell Res.* **2016**, *340*, 71–80. [[CrossRef](#)]
52. Rahman, M.S.; Rana, M.; Spitzhorn, L.-S.; Akhtar, N.; Hasan, M.Z.; Choudhury, N.; Fehm, T.; Czernuszka, J.T.; Adjaye, J.; Asaduzzaman, S.M. Fabrication of biocompatible porous scaffolds based on hydroxyapatite/collagen/chitosan composite for restoration of defected maxillofacial mandible bone. *Prog. Biomater.* **2019**, *8*, 137–154. [[CrossRef](#)]
53. Dreissig, I.; Machill, S.; Salzer, R.; Krafft, C. Quantification of brain lipids by FTIR spectroscopy and partial least squares regression. *Spectrochim. Acta Part A Mol. Biomol. Spectrosc.* **2009**, *71*, 2069–2075. [[CrossRef](#)]
54. Naseer, K.; Ali, S.; Qazi, J. ATR-FTIR spectroscopy as the future of diagnostics: A systematic review of the approach using bio-fluids. *Appl. Spectrosc. Rev.* **2021**, *56*, 85–97. [[CrossRef](#)]
55. Fung, M.F.K.; Senterman, M.K.; Mikhael, N.Z.; Lacelle, S.; Wong, P.T. Pressure-tuning fourier transform infrared spectroscopic study of carcinogenesis in human endometrium. *Biospectroscopy* **1996**, *2*, 155–165. [[CrossRef](#)]
56. Balan, V.; Mihai, C.T.; Cojocaru, F.D.; Uritu, C.M.; Dodi, G.; Botezat, D.; Gardikiotis, I. Vibrational spectroscopy fingerprinting in medicine: From molecular to clinical practice. *Materials* **2019**, *12*, 2884. [[CrossRef](#)]
57. Müller, G.; Schöpfer, C.; Vos, H.; Kharazipour, A.; Polle, A. FTIR-ATR spectroscopic analyses of changes in wood properties during particle-and fibreboard production of hard-and softwood trees. *BioResources* **2009**, *4*, 49–71. [[CrossRef](#)]
58. Asare, S. *Synthesis, Characterization and Molecular Dynamic Simulations of Aqueous Choline Chloride Deep Eutectic Solvents*; South Dakota State University: Brookings, SD, USA, 2018.
59. Suzuki, T.; Sato, T.; Zhang, J.; Kanao, M.; Higuchi, M.; Maki, H. Electrochemically switchable photoluminescence of an anionic dye in a cationic metallo-supramolecular polymer. *J. Mater. Chem. C* **2016**, *4*, 1594–1598. [[CrossRef](#)]

60. Trivedi, M.; Branton, A.; Trivedi, D.; Shettigar, H.; Bairwa, K.; Jana, S. Fourier transform infrared and ultraviolet-visible spectroscopic characterization of biofield treated salicylic acid and sparfloxacin. *Nat. Prod. Chem. Res.* **2015**, *5*, 1–6. [[CrossRef](#)]
61. Jamil, B.; Habib, H.; Abbasi, S.A.; Ihsan, A.; Nasir, H.; Imran, M. Development of cefotaxime impregnated chitosan as nano-antibiotics: De novo strategy to combat biofilm forming multi-drug resistant pathogens. *Front. Microbiol.* **2016**, *7*, 330. [[CrossRef](#)]
62. Baisya, S.S. Coordination Chemistry of Pteridine Ligands with Transition and d10 Metals. Ph.D. Dissertation, University of North Bengal, West Bengal, India, 2016.
63. Xiang, Z.; Gao, W.; Chen, L.; Lan, W.; Zhu, J.Y.; Runge, T. A comparison of cellulose nanofibrils produced from *Cladophora glomerata* algae and bleached eucalyptus pulp. *Cellulose* **2016**, *23*, 493–503. [[CrossRef](#)]
64. Peng, N.; Huang, D.; Gong, C.; Wang, Y.; Zhou, J.; Chang, C. Controlled arrangement of nanocellulose in polymeric matrix: From reinforcement to functionality. *ACS Nano* **2020**, *14*, 16169–16179. [[CrossRef](#)]
65. Tan, Z.; Chen, S.; Peng, X.; Zhang, L.; Gao, C. Polyamide membranes with nanoscale Turing structures for water purification. *Science* **2018**, *360*, 518–521. [[CrossRef](#)]
66. Hamouda, R.A.; Hussein, M.H.; Elhadary, A.M.A.; Abuelmagd, M.A. Extruded polysaccharide/protein matrix from *Arthrospira platensis* cultures mediated silver nanoparticles biosynthesis and capping. *Appl. Nanosci.* **2020**, *10*, 3839–3855. [[CrossRef](#)]
67. Rajeshkumar, S.; Tharani, M.; Rajeswari, V.D.; Alharbi, N.S.; Kadaikunnan, S.; Khaled, J.M.; Govindarajan, M. Synthesis of greener silver nanoparticle-based chitosan nanocomposites and their potential antimicrobial activity against oral pathogens. *Green Process. Synth.* **2021**, *10*, 658–665. [[CrossRef](#)]
68. Liu, G.Q.; Pan, X.J.; Li, J.; Li, C.; Ji, C.L. Facile preparation and characterization of anatase TiO₂/nanocellulose composite for photocatalytic degradation of methyl orange. *J. Saudi Chem. Soc.* **2021**, *25*, 101383. [[CrossRef](#)]
69. Ullah, S.; Ahmad, A.; Subhan, F.; Jan, A.; Raza, M.; Khan, A.U.; Rahman, A.-U.; Khan, U.A.; Tariq, M.; Yuan, Q. Tobramycin mediated silver nanospheres/graphene oxide composite for synergistic therapy of bacterial infection. *J. Photochem. Photobiol. B Biol.* **2018**, *183*, 342–348. [[CrossRef](#)] [[PubMed](#)]
70. Dong, Y.Y.; Fu, L.H.; Liu, S.; Ma, M.G.; Wang, B. Silver-reinforced cellulose hybrids with enhanced antibacterial activity: Synthesis, characterization, and mechanism. *RSC Adv.* **2015**, *5*, 97359–97366. [[CrossRef](#)]
71. Sasi, S.; Krishna, C.A.; Sugunan, S.K.; Chandran, A.; Nair, P.R.; Subramanian, K.R.V.; Mathew, S. Low cost, high efficiency flexible supercapacitor electrodes made from areca nut husk nanocellulose and silver nanoparticle embedded polyaniline. *RSC Adv.* **2021**, *11*, 29564–29575. [[CrossRef](#)]
72. Nisizawa, K. Mode of action of cellulases. *J. Ferment. Technol.* **1973**, *51*, 267–304.
73. Fan, L.; Zhang, H.; Gao, M.; Zhang, M.; Liu, P.; Liu, X. Cellulose nanocrystals/silver nanoparticles: In-situ preparation and application in PVA films. *Holzforchung* **2020**, *74*, 523–528. [[CrossRef](#)]
74. Bai, L.; Liu, Y.; Ding, A.; Ren, N.; Li, G.; Liang, H. Fabrication and characterization of thin-film composite (TFC) nanofiltration membranes incorporated with cellulose nanocrystals (CNCs) for enhanced desalination performance and dye removal. *Chem. Eng. J.* **2019**, *358*, 1519–1528. [[CrossRef](#)]
75. Shin, J.U.; Gwon, J.; Lee, S.Y.; Yoo, H.S. Silver-incorporated nanocellulose fibers for antibacterial hydrogels. *ACS Omega* **2018**, *3*, 16150–16157. [[CrossRef](#)]
76. Abo-Elmagd, R.A.; Hussein, M.H.; Hamouda, R.A.; Shalan, A.E.; Abdelrazak, A. Statistical optimization of photo-induced biofabrication of silver nanoparticles using the cell extract of *Oscillatoria limnetica*: Insight on characterization and antioxidant potentiality. *RSC Adv.* **2020**, *10*, 44232–44246. [[CrossRef](#)] [[PubMed](#)]
77. Hamouda, R.A.; Hussein, M.H.; Abo-Elmagd, R.A.; Bawazir, S.S. Synthesis and biological characterization of silver nanoparticles derived from the cyanobacterium *Oscillatoria limnetica*. *Sci. Rep.* **2019**, *9*, 13071. [[CrossRef](#)] [[PubMed](#)]
78. Hamouda, R.A.; El Maksoud, A.I.A.; Wageed, M.; Alotaibi, A.S.; Elebeedy, D.; Khalil, H.; Hassan, A.; Abdella, A. Characterization and anticancer activity of biosynthesized Au/cellulose nanocomposite from *Chlorella vulgaris*. *Polymers* **2021**, *13*, 3340. [[CrossRef](#)]
79. Prathapan, R.; Thapa, R.; Garnier, G.; Tabor, R.F. Modulating the zeta potential of cellulose nanocrystals using salts and surfactants. *Colloids Surf. A Physicochem. Eng. Asp.* **2016**, *509*, 11–18. [[CrossRef](#)]
80. Asad, M.; Saba, N.; Asiri, A.M.; Jawaid, M.; Indarti, E.; Wanrosli, W.D. Preparation and characterization of nanocomposite films from oil palm pulp nanocellulose/poly (Vinyl alcohol) by casting method. *Carbohydr. Polym.* **2018**, *191*, 103–111. [[CrossRef](#)]
81. de Oliveira, A.R.; Molina, E.F.; de Castro Mesquita, P.; Fonseca, J.L.C.; Rossanezi, G.; de Freitas Fernandes-Pedrosa, M.; de Oliveira, A.G.; da Silva-Júnior, A.A. Structural and thermal properties of spray-dried methotrexate-loaded biodegradable microparticles. *J. Therm. Anal. Calorim.* **2013**, *112*, 555–565. [[CrossRef](#)]
82. Rantuch, P.; Chrebet, T.O.M.Á.Š. Thermal decomposition of cellulose insulation. *Cellul. Chem. Technol.* **2014**, *48*, 461–467.
83. Zhu, P.; Ma, D. Double cold crystallization peaks of poly (ethylene terephthalate)—1. Samples isothermally crystallized at low temperature. *Eur. Polym. J.* **1997**, *33*, 1817–1818. [[CrossRef](#)]
84. Mou, K.; Li, J.; Wang, Y.; Cha, R.; Jiang, X. 2, 3-Dialdehyde nanofibrillated cellulose as a potential material for the treatment of MRSA infection. *J. Mater. Chem. B* **2017**, *5*, 7876–7884. [[CrossRef](#)]
85. Khulbe, K.C.; Matsuura, T. Membrane applications. In *Nanotechnology in Membrane Processes*; Springer: Cham, Switzerland, 2021; pp. 199–343. [[CrossRef](#)]
86. Tyagi, P.; Mathew, R.; Opperman, C.H.; Jameel, H.; Gonzalez, R.W.; Lucia, L.A.; Hubbe, M.A.; Pal, L. High-strength antibacterial chitosan–cellulose nanocrystal composite tissue paper. *Langmuir* **2018**, *35*, 104–112. [[CrossRef](#)] [[PubMed](#)]

87. Nguyen, H.-L.; Jo, Y.K.; Cha, M.; Cha, Y.J.; Yoon, D.K.; Sanandiya, N.D.; Prajatelista, E.; Oh, D.X.; Hwang, D.S. Mussel-inspired anisotropic nanocellulose and silver nanoparticle composite with improved mechanical properties, electrical conductivity and antibacterial activity. *Polymers* **2016**, *8*, 102. [[CrossRef](#)]
88. Marambio-Jones, C.; Hoek, E. A review of the antibacterial effects of silver nanomaterials and potential implications for human health and the environment. *J. Nanoparticle Res.* **2010**, *12*, 1531–1551. [[CrossRef](#)]
89. Farooq, A.; Patoary, M.K.; Zhang, M.; Mussana, H.; Li, M.; Naeem, M.A.; Mushtaq, M.; Farooq, A.; Liu, L. Cellulose from sources to nanocellulose and an overview of synthesis and properties of nanocellulose/zinc oxide nanocomposite materials. *Int. J. Biol. Macromol.* **2020**, *154*, 1050–1073. [[CrossRef](#)]
90. Martins, N.C.T.; Freire, C.; Pinto, R.; Fernandes, S.C.M.; Neto, C.; Silvestre, A.; Causio, J.; Baldi, G.; Sadocco, P.; Trindade, T. Electrostatic assembly of Ag nanoparticles onto nanofibrillated cellulose for antibacterial paper products. *Cellulose* **2012**, *19*, 1425–1436. [[CrossRef](#)]
91. Percival, S.L.; Bowler, P.G.; Russell, D. Bacterial resistance to silver in wound care. *J. Hosp. Infect.* **2005**, *60*, 1–7. [[CrossRef](#)]
92. El-Abd, N.M.; Hamouda, R.A.; Al-Shaikh, T.M.; Abdel-Hamid, M.S. Influence of biosynthesized silver nanoparticles using red alga *Corallina elongata* on broiler chicks' performance. *Green Process. Synth.* **2022**, *11*, 238–253. [[CrossRef](#)]
93. Hamouda, R.A.; Abd El-Mongy, M.; Eid, K.F. Comparative study between two red algae for biosynthesis silver nanoparticles capping by SDS: Insights of characterization and antibacterial activity. *Microb. Pathog.* **2019**, *129*, 224–2321. [[CrossRef](#)]
94. Yin, I.X.; Zhao, I.S.; Mei, M.L.; Lo, E.C.M.; Tangm, J.; Li, Q.; So, L.Y.; Chu, C.H. Synthesis and Characterization of Fluoridated Silver Nanoparticles and Their Potential as a Non-Staining Anti-Caries Agent. *Int. J. Nanomed.* **2020**, *15*, 3207–3215. [[CrossRef](#)]
95. dos Santos, V.E.; Filho, A.V.; Ribeiro Targino, A.G.; Pelagio Flores, M.A.; Galembeck, A.; Caldas, A.F. A New “Silver-Bullet” to Treat Caries in Children—Nano Silver Fluoride: A Randomised Clinical Trial. *J. Dent.* **2014**, *42*, 945–951. [[CrossRef](#)]
96. Vijayakumar, M.; Sabari Lavanya, S.J.; Ponnudurai Arangannal, J.J.; Aarthi, A.S. Nano Silver Fluoride-Overview. *Eur. J. Mol. Clin. Med.* **2020**, *7*, 6573–6580.
97. Widakdo, J.; Wu, P.W.; Austria, H.F.M.; Hung, W.S.; Yu, P.J.; Wang, C.F.; Hu, C.C.; Lee, K.R.; Lai, J.Y. Dual functional GO-Ag incorporated nanocomposite pervaporation membrane with alcohol dehydration performance and enhanced antibacterial property. *Mater. Today Chem.* **2022**, *24*, 100985. [[CrossRef](#)]
98. Widakdo, J.; Chen, T.M.; Lin, M.C.; Wu, J.H.; Lin, T.L.; Yu, P.J.; Hung, W.S.; Lee, K.R. Evaluation of the Antibacterial Activity of Eco-Friendly Hybrid Composites on the Base of Oyster Shell Powder Modified by Metal Ions and LLDPE. *Polymers* **2022**, *14*, 3001. [[CrossRef](#)] [[PubMed](#)]
99. Selvaraj, P.; Neethu, E.; Rathika, P.; Jayaseeli, J.P.R.; Jermy, B.R.; AbdulAzeez, S.; Dhas, T.S. Antibacterial potentials of methanolic extract and silver nanoparticles from marine algae. *Biocatal. Agric. Biotechnol.* **2020**, *28*, 101719. [[CrossRef](#)]
100. Aboelfetoh, E.F.; El-Shenody, R.A.; Ghobara, M.M. Eco-friendly synthesis of silver nanoparticles using green algae (*Caulerpa serrulata*): Reaction optimization, catalytic and antibacterial activities. *Environ. Monit. Assess.* **2017**, *189*, 349. [[CrossRef](#)]
101. Kathiraven, T.; Sundaramanickam, A.; Shanmugam, N.; Balasubramanian, T. Green synthesis of silver nanoparticles using marine algae *Caulerpa racemosa* and their antibacterial activity against some human pathogens. *Appl. Nanosci.* **2015**, *5*, 499–504. [[CrossRef](#)]
102. Borah, D.; Das, N.; Das, N.; Bhattacharjee, A.; Sarmah, P.; Ghosh, K.; Bhattacharjee, C.R. Alga-mediated facile green synthesis of silver nanoparticles: Photophysical, catalytic and antibacterial activity. *Appl. Organomet. Chem.* **2020**, *34*, e5597. [[CrossRef](#)]
103. Venkatesan, J.; Kim, S.K.; Shim, M.S. Antimicrobial, antioxidant, and anticancer activities of biosynthesized silver nanoparticles using marine algae *Ecklonia cava*. *Nanomaterials* **2016**, *6*, 235. [[CrossRef](#)]
104. Garza-Cervantes, J.A.; Mendiola-Garza, G.; de Melo, E.M.; Dugmore, T.I.; Matharu, A.S.; Morones-Ramirez, J.R. Antimicrobial activity of a silver-microfibrillated cellulose biocomposite against susceptible and resistant bacteria. *Sci. Rep.* **2020**, *10*, 7281. [[CrossRef](#)]
105. Thiagamani, S.M.K.; Rajini, N.; Siengchin, S.; Rajulu, A.V.; Hariram, N.; Ayrilmis, N. Influence of silver nanoparticles on the mechanical, thermal and antimicrobial properties of cellulose-based hybrid nanocomposites. *Compos. Part B Eng.* **2019**, *165*, 516–525. [[CrossRef](#)]
106. Adepu, S.; Khandelwal, M. Broad-spectrum antimicrobial activity of bacterial cellulose silver nanocomposites with sustained release. *J. Mater. Sci.* **2018**, *53*, 1596–1609. [[CrossRef](#)]
107. Audtarat, S.; Hongsachart, P.; Dasri, T.; Chio-Srichan, S.; Soontaranon, S.; Wongsinlatam, W.; Sompech, S. Green synthesis of silver nanoparticles loaded into bacterial cellulose for antimicrobial application. *Nanocomposites* **2022**, *2018*, 34–46. [[CrossRef](#)]

Disclaimer/Publisher's Note: The statements, opinions and data contained in all publications are solely those of the individual author(s) and contributor(s) and not of MDPI and/or the editor(s). MDPI and/or the editor(s) disclaim responsibility for any injury to people or property resulting from any ideas, methods, instructions or products referred to in the content.